

Semantics-aware Motion Retargeting with Vision-Language Models

Haodong Zhang^{1*} Zhike Chen^{1*} Haocheng Xu¹ Lei Hao² Xiaofei Wu²
 Songcen Xu² Zhensong Zhang² Yue Wang¹ Rong Xiong^{1†}
¹Zhejiang University ²Huawei Noah’s Ark Lab

Abstract

Capturing and preserving motion semantics is essential to motion retargeting between animation characters. However, most of the previous works neglect the semantic information or rely on human-designed joint-level representations. Here, we present a novel *Semantics-aware Motion reTargeting (SMT)* method with the advantage of vision-language models to extract and maintain meaningful motion semantics. We utilize a differentiable module to render 3D motions. Then the high-level motion semantics are incorporated into the motion retargeting process by feeding the vision-language model with the rendered images and aligning the extracted semantic embeddings. To ensure the preservation of fine-grained motion details and high-level semantics, we adopt a two-stage pipeline consisting of skeleton-aware pre-training and fine-tuning with semantics and geometry constraints. Experimental results show the effectiveness of the proposed method in producing high-quality motion retargeting results while accurately preserving motion semantics. Project page can be found at <https://sites.google.com/view/smtnet>.

1. Introduction

3D animation characters have extensive application in animation production, virtual reality, and various other domains. These characters are animated using motion data, resulting in lifelike and immersive animations. Nevertheless, acquiring motion data for each character can be a costly endeavor. Therefore, the ability to retarget existing motion data for new characters holds immense importance. The goal of motion retargeting is to transfer existing motion data to new characters following motion feature extraction and integration processes, which ensure the preservation of the original motion’s characteristics.

Semantics encompasses the meaningful and contextually relevant information conveyed in motion and plays a critical role in ensuring the realism and vividness of the anima-

*These authors contributed equally to this work

†Corresponding author: rxiong@zju.edu.cn

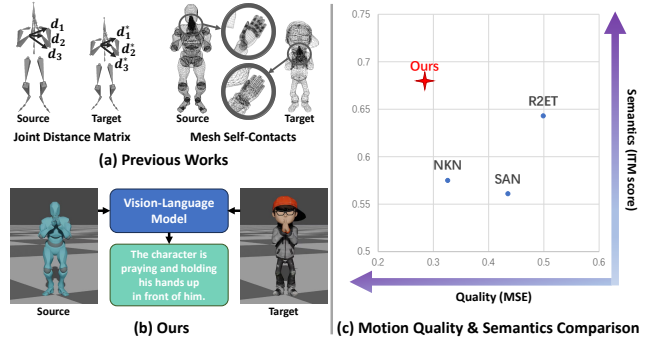


Figure 1. Comparison with previous motion retargeting methods. (a) Previous works rely on human-designed joint distance matrix [29] or self-contacts between mesh vertices [27] to ensure semantics preservation. (b) Ours work enforces human-level motion semantics consistency with the extensive knowledge of vision-language models. (c) Comparison of motion quality and semantics preservation on the Mixamo dataset [1]. Our method achieves the best motion quality and semantics consistency.

tion characters. Preservation of motion semantics can enhance the efficiency of motion retargeting by reducing the need for time-consuming manual adjustments and refinements. However, previous methods [2, 16, 26] are mainly based on retargeting of joint positions and make less use of the extraction of semantic information. They focus on trajectory-level motion retargeting with few attention to motion semantics. Consequently, this leads to a significant loss of motion semantics and necessitates the labor-intensive intervention of animation artists for manual trajectory adjustments. Recent advancements have introduced self-contacts [27] and joint distance matrices [29] as the representation of motion semantics. Nevertheless, self-contacts are not applicable to non-contact semantics and require intricate vertex correspondence. The human-designed joint distance matrices primarily focus on joint relative relationships and still lack consideration of high-level semantic information.

To address the intricate task of capturing and preserving motion semantics, we introduce a new perspective: the most general and comprehensive form of motion semantics is human-level natural language, reflecting the user’s intu-

itive understanding of motion. However, the main challenge of human-level motion semantics representation lies in the scarcity of labelled data. It is difficult and expensive to label sufficient semantic textual descriptions for motion data.

In this paper, we introduce the incorporation of robust, state-of-the-art vision-language models to provide semantic guidance to the motion retargeting network. In the absence of labelled semantic data, we leverage the capabilities of a vision-language model to serve as a semantic supervisor in an unsupervised manner, which can extract motion semantics in a more intuitive way, as illustrated in Fig. 1. This approach offers a solution to the challenge of the limited availability of labelled semantic datasets for motion retargeting. To establish a connection between the vision-language model and motion semantics extraction, we employ the differentiable skinning and rendering modules to translate 3D motions into image sequences. Subsequently, we adopt visual question answering with guiding questions to inquire about the most relevant motion semantics from the vision-language model.

To guarantee the preservation of motion semantics during motion retargeting, we introduce a semantics consistency loss that enforces the semantic embeddings of the retargeted motion to closely align with those of the source motion. For dense semantic supervision and computational efficiency, we utilize latent features extracted by the vision-language model as the semantic embeddings instead of textual descriptions. To alleviate the non-linearity of the semantics consistency loss, we introduce a two-stage training approach. We categorize motion information into two distinct levels: the skeletal level and the semantic level. Our approach involves pre-training the motion retargeting network at the skeletal level, which is then further refined and fine-tuned at the semantic level with the power of vision-language models. To the best of our knowledge, we are the first to leverage the extensive capability of vision-language models for the task of semantics-aware motion retargeting.

To summarize, the contributions of our work include:

- We introduce an innovative framework that leverages the expertise of vision-language models as a semantic supervisor to tackle the challenge of limited labelled semantic data for the task of motion retargeting.
- We propose to use differentiable skinning and rendering to translate from the motion domain to the image domain and perform guiding visual question answering to obtain human-level semantic representation.
- We design a semantics consistency loss to maintain motion semantics and introduce an effective two-stage training pipeline consisting of pre-training at the skeletal level and fine-tuning at the semantic level.
- Our model achieves state-of-the-art performance in the challenging task of semantics-aware motion retargeting, delivering exceptional performance marked by high-

quality motion and superior semantics consistency.

2. Related Works

Optimization-based Motion Retargeting. Motion retargeting is a technique to adapt existing motion data from a source character to a target character with different bone proportions, mesh skins, and skeletal structures. Early works formulate motion retargeting as a constrained optimization problem [4, 6, 11, 21]. Gleicher *et al.* [6] introduced a motion retargeting method, which identifies motion features as constraints and computes an adapted motion using a space-time constraint solver to preserve the desirable qualities. Lee *et al.* [11] proposed a method to adapt existing motion of a human-like character to have the desired features with specified constraints and combined a hierarchical curve fitting technique with inverse kinematics. Nonetheless, these methods necessitate the tedious and time-consuming process of formulating human-designed constraints for specific motion sequences.

Learning-based Motion Retargeting. With the rise of deep learning, researchers have been developing learning-based motion retargeting methods in recent years [2, 9, 16, 26, 27, 29]. Villegas *et al.* [26] presented a recurrent neural network architecture, which incorporates a forward kinematics layer and cycle consistency loss for unsupervised motion retargeting. Aberman *et al.* [2] designed a skeleton-aware network with differentiable convolution, pooling, and unpooling operators to transform various homeomorphic skeletons into a primary skeleton for cross-structural motion retargeting. However, these methods tend to concentrate on trajectory-level motion retargeting with limited consideration for motion semantics, which often results in a notable loss of motion semantics and increase the heavy burden of manual adjustments to the trajectories. To address these problems, Zhang *et al.* [29] presented a residual retargeting network that uses a skeleton-aware module to preserve motion semantics and a shape-aware module to reduce interpenetration and contact missing. While this method successfully preserves joint relative relationships, it still falls short in addressing high-level motion semantics.

Vision-Language Models. Vision-language models have empowered various vision-language tasks, including visual question answering and image captioning. Tevet *et al.* [23] introduced a human motion generation model that aligns the latent space with that of the Contrastive Language-Image Pre-training (CLIP) model. Li *et al.* [13] proposed a pre-training strategy from off-the-shelf frozen pre-trained image encoders and frozen large language models for vision-to-language generative learning. Zhu *et al.* [31] presented a vision-language model, which uses one projection layer to align a frozen visual encoder with a frozen advanced large language models (LLM). However, these efforts primarily concentrate on vision-language tasks, leaving the question

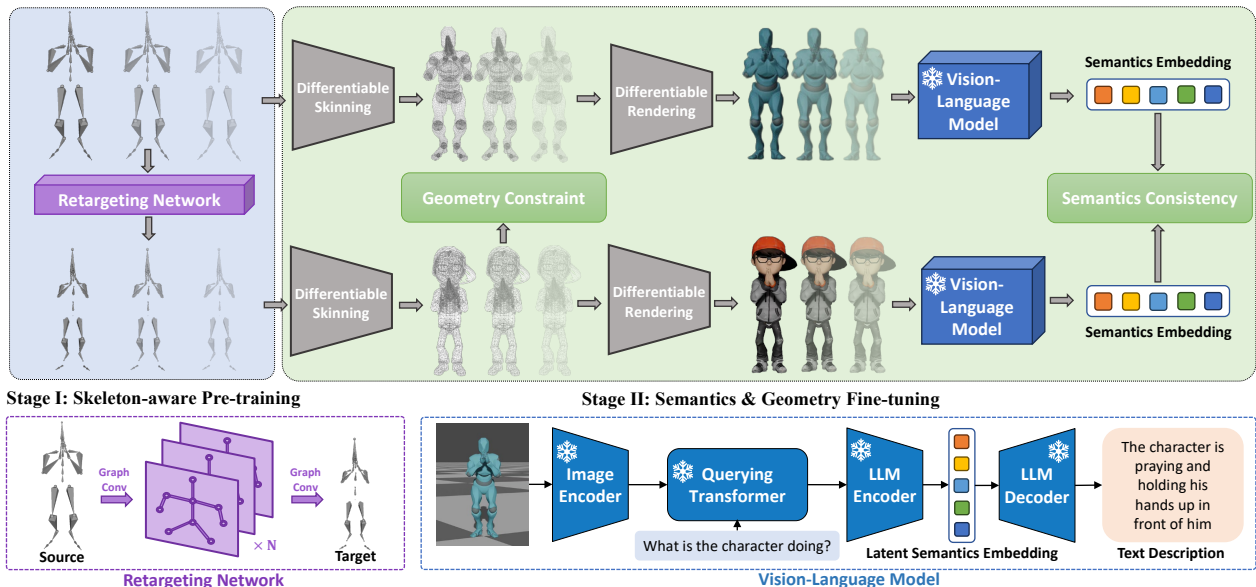


Figure 2. **Model Architecture.** Our semantics-aware motion retargeting framework employs a two-stage pipeline. Initially, the retargeting network consisting of multiple spatial-temporal graph convolution layers is trained at the skeletal level to establish a base model. Subsequently, this model undergoes further refinement and fine-tuning at the semantic level by the alignment of latent semantic embeddings of the source and target, leveraging the extensive knowledge of vision-language models. The latent semantic embedding is extracted by guiding visual question answering. Additionally, the geometry constraints are also enforced during fine-tuning to avoid interpenetration.

of how to effectively employ vision-language models to guide motion retargeting as an open and unexplored area.

Human motion synthesis. Human motion synthesis is a domain related to motion retargeting, which aims to synthesize realistic and lifelike human motions from random noise or other inputs with generative networks. Guo *et al.* [7] proposed to generate human motion sequences based on action type. Guo *et al.* [8] presented a temporal variational auto-encoder to synthesize human motions from text input. Tevet *et al.* [24] introduced a diffusion-based generative model for human motion generation. As comparison, we focus on the task of motion retargeting, where existing motion data is transferred from a source character to a target character.

3. Method

3.1. Overview

We present a novel semantic-aware motion retargeting method, as illustrated in Fig 2. In contrast to previous methods that neglect motion semantics [2, 16, 26] or rely on human-designed joint-level representations [29], our approach integrates natural language descriptions from vision-language models to offer an explicit and comprehensive semantic representation of character motions, thereby maintaining the preservation of semantic consistency.

Task definition. Given a source motion sequence, consisting of the skeleton motion and its associated skinning geometry, as well as a target character in the reference pose (e.g.,

T-pose), the objective of motion retargeting is to generate the target motion while preserving crucial motion characteristics, such as joint trajectory similarity and motion semantics, and satisfying geometry constraints.

Graph representation. The skeleton motion sequence can be modelled as a sequence of graphs according to the skeleton hierarchy where each node corresponds to a joint and each edge represents a directed connection between joints. Assume that the motion sequence has T frames in total and the animation characters have N nodes and M edges. In our approach, we consider motion data as node features $\mathbf{Q} \in \mathbb{R}^{T \times N \times 9}$, which encompass the 6D joint rotation representation [30] and 3D joint positions. Additionally, we utilize skeleton hierarchy information as edge features $\mathbf{E} \in \mathbb{R}^{M \times 3}$, which consists of the 3D position offset between each joint and its parent joint.

Two-stage training. The motion of animation characters can be divided into skeletal movements and skinned movements, represented by skeletal joints and skinned vertices respectively. The skinned movements can be derived from the skeletal movements through the linear blend skinning algorithm [12]. Therefore, motion retargeting at the skeletal level can effectively downscale the data and reduce the complexity of the problem. However, this simplification process can lead to the loss of motion semantics and violations of geometry constraints. To address these issues, we employ a two-stage pipeline. Initially, we pre-train a skeleton-aware network to ensure a general initialization for motion retar-

getting without considering motion semantics and geometry constraints. Subsequently, we fine-tune the pre-trained network for each source-target character pair with the vision-language model to maintain semantic consistency and enforce geometry constraints to prevent interpenetrations.

3.2. Skeleton-aware Pre-training

Retargeting network. We propose a retargeting network consisting of a graph motion encoder and a graph motion decoder for motion retargeting. The motion encoder \mathcal{F}_θ encodes the motion data \mathbf{Q}_A of the source character A into the latent motion embedding \mathbf{Z}_A . Then, the motion decoder \mathcal{F}_ϕ generates the joint angles \mathbf{Q}_B of the target character B based on the latent features. Both the motion encoder and decoder are composed of multiple graph convolutions. More details are available in the supplementary materials.

$$\begin{aligned}\mathbf{Z}_A &= \mathcal{F}_\theta(\mathbf{Q}_A, \mathbf{E}_A) \\ \mathbf{Q}_B &= \mathcal{F}_\phi(\mathbf{Z}_A, \mathbf{E}_B)\end{aligned}\quad (1)$$

In the first phase, we train the motion encoder and decoder at the skeletal level to establish a robust initialization for motion retargeting. Following the unsupervised learning setting in [26], we train the network with the reconstruction loss, cycle consistency loss, adversarial loss, and joint relationship loss. The overall objective function for skeleton-aware pre-training is defined as follows:

$$\mathcal{L}_{skel} = \lambda_r \mathcal{L}_{rec} + \lambda_c \mathcal{L}_{cyc} + \lambda_a \mathcal{L}_{adv} + \lambda_j \mathcal{L}_{jdm} \quad (2)$$

The reconstruction loss \mathcal{L}_{rec} encourages the retargeted motion to match the source motion when the target character is the same as the source character. Let $\mathbf{Q}_{A,t}$ be the motion data of source character A at frame t , and $\hat{\mathbf{Q}}_{A,t}^{rec}$ be the reconstructed motion. Then \mathcal{L}_{rec} is defined as:

$$\mathcal{L}_{rec} = \sum_t \left\| \hat{\mathbf{Q}}_{A,t}^{rec} - \mathbf{Q}_{A,t} \right\|_2^2 \quad (3)$$

The cycle consistency loss \mathcal{L}_{cyc} promotes the consistency of retargeted motion from the source character A to the target character B and then back to the source character A, ensuring it remains in line with the original motion. Let $\hat{\mathbf{Q}}_{A,t}^{cyc}$ represent the retargeted motion. Then \mathcal{L}_{cyc} is defined as:

$$\mathcal{L}_{cyc} = \sum_t \left\| \hat{\mathbf{Q}}_{A,t}^{cyc} - \mathbf{Q}_{A,t} \right\|_2^2 \quad (4)$$

The adversarial loss \mathcal{L}_{adv} is calculated by a discriminator network, which utilizes the unpaired data of the target character to learn how to distinguish whether the motions are real or fake. Let \mathcal{F}_γ be the discriminator network, and $\mathbf{Q}_{B,t}$ be the retargeted motion at frame t . Then it is defined as:

$$\mathcal{L}_{adv} = \sum_t \log(1 - \mathcal{F}_\gamma(\mathbf{Q}_{B,t})) \quad (5)$$

The joint relationship loss \mathcal{L}_{jdm} is calculated by the joint distance matrix (JDM) $\mathbf{D} \in \mathbb{R}^{N \times N}$, which represents the relative positional relationships of the joints. The element $d_{i,j}$ of \mathbf{D} represents the Euclidean distance between joint i and joint j . We extract the joint distance matrix from the target character and compare it with the source character. Then \mathcal{L}_{jdm} is defined as:

$$\mathcal{L}_{jdm} = \sum_t \left\| \eta(\mathbf{D}_{A,t}) - \eta(\mathbf{D}_{B,t}) \right\|_2^2 \quad (6)$$

where $\eta(\cdot)$ is an L1 normalization performed on each row of the distance matrix. This normalization operation eliminates the difference in bone length to some extent.

3.3. Semantics & Geometry Fine-tuning

In the second phase, we fine-tune the pre-trained retargeting network for each source-target character pair to preserve motion semantics and satisfy geometry constraints. The motion semantics is maintained by the semantics consistency loss, which aligns the semantic embeddings extracted from a vision-language model for both the source and target. Additionally, the geometry constraint is satisfied by minimizing the interpenetration loss. The overall objective function for fine-tuning is outlined as follows:

$$\mathcal{L}_{fine} = \lambda_s \mathcal{L}_{sem} + \lambda_p \mathcal{L}_{pen} \quad (7)$$

Differentiable skinning & rendering. To make the fine-tuning process differentiable for gradient back-propagation, we first use the differentiable linear blend skinning algorithm [12], denoted as \mathcal{F}_{lbs} , to transform the target joint angles \mathbf{Q}_B into skinned motions \mathbf{V}_B , represented by 3D mesh vertices. Subsequently, we employ the differentiable projection function \mathcal{F}_{proj} as introduced in [18] to convert the skinned motions into 2D images \mathbf{I}_B . A limitation for the differentiable rendering process is that when projecting the 3D skinned mesh onto 2D images, the depth information is lost. To obtain a comprehensive semantic representation of the motion, we render the character from multiple perspectives and then combine the extracted features, following the Non-rigid Shape Fitting task in [18].

$$\begin{aligned}\mathbf{I}_A &= \mathcal{F}_{proj}(\mathcal{F}_{lbs}(\mathbf{Q}_A)) \\ \mathbf{I}_B &= \mathcal{F}_{proj}(\mathcal{F}_{lbs}(\mathbf{Q}_B))\end{aligned}\quad (8)$$

Frozen vision-language model. To obtain an explicit and reliable semantic feature of the motion, we employ a frozen vision-language model as our semantic supervisor. Current 3D vision-language datasets [3, 32] mainly focus on the occupation or the segmentation of the object in a spatial scene like rooms, and thus the state-of-the-art 3D vision-language models [32] lack prior knowledge relevant to animation characters. In contrast, 2D vision-language models achieve better results in semantic tasks, such as image captioning, visual question answering and image-text

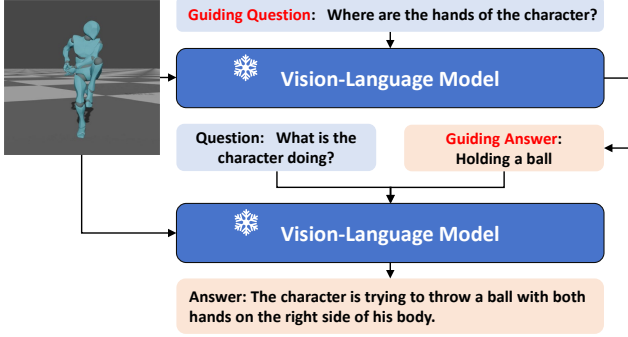


Figure 3. An example of guiding visual question answering.

retrieval, and provides cleaner and richer semantics [28]. Therefore, we utilize a frozen 2D vision-language model to extract latent embeddings of motion semantics. The frozen 2D vision-language model employed in our work is BLIP-2 [14], which incorporates a lightweight querying transformer as a bridge between the off-the-shelf frozen pre-trained image encoder and the frozen large language model.

Prompt design. Since the vision-language model has the capability to extract rich information from images, it is possible that the extracted features might contain redundant details, such as the appearance of the character. To guide the vision-language model to obtain semantic embedding relevant to character motions, we adopt a guiding visual question answering approach for motion semantics extraction, as depicted in Fig. 3. We believe that there is a strong correlation between motion semantics and hand movements. To acquire a more comprehensive description of the motion, we initially provide a guiding question to BLIP-2: “*Where are the hands of the character?*”. Subsequently, we introduce a new question and combine it with the first answer as the input to BLIP-2: “[*The answers to the first question generated by the vision-language model*] *What is the character in the image doing?*”. For more details, please refer to the supplementary materials.

Latent semantic embedding. We opt to align the latent semantic embeddings of the source and target generated by the vision-language model rather than relying on textual descriptions, specifically leveraging the encoder output of the large language model. This approach enables us to acquire a more accurate and denser representation, while also mitigating computational costs and the non-linearity of the training objective caused by the large number of parameters of the vision-language model. Let \mathbf{E}_A and \mathbf{E}_B be the latent semantic embeddings of the source and target motions, \mathcal{F}_ω be the frozen pre-trained image encoder, \mathcal{F}_σ be the frozen querying transformer, \mathcal{F}_ψ be the encoder of the frozen large language model, and *context* be the question.

$$\begin{aligned} \mathbf{E}_A &= \mathcal{F}_\psi(\mathcal{F}_\sigma(\mathcal{F}_\omega(\mathbf{I}_A), \text{context})) \\ \mathbf{E}_B &= \mathcal{F}_\psi(\mathcal{F}_\sigma(\mathcal{F}_\omega(\mathbf{I}_B), \text{context})) \end{aligned} \quad (9)$$

Fine-tuning with semantics consistency. As illustrated in Fig. 2, our approach aligns the latent semantic embeddings of both the source and target motions in an unsupervised manner, ensuring a high degree of semantic consistency in the retargeted results. The semantics consistency loss \mathcal{L}_{sem} is calculated using the mean square error and it is defined as follows:

$$\mathcal{L}_{sem} = \sum_t \|\mathbf{E}_{A,t} - \mathbf{E}_{B,t}\|_2^2 \quad (10)$$

Fine-tuning with geometry constraints. From our observations, most interpenetration problems occur between the limbs and the main body. To address this, we incorporate the signed distance field between the limb vertices and the body mesh as the interpenetration loss. First, we convert the skeleton motion output from the network into mesh vertices using the linear blend skinning method [12]. Then, the interpenetration loss is defined as follows:

$$\mathcal{L}_{pen} = \sum_t ReLU(-\Phi_{b,t}(\mathbf{V}_{l,t})) \quad (11)$$

where Φ_b indicates the signed distance field function, \mathbf{V}_l is the vertices of the limbs. If the vertex locates inside the body, the value of the function is less than zero. Therefore, we use the *ReLU* function to penalize the inner vertices.

4. Experiments

4.1. Settings

Datasets. We train and evaluate our method on the Mixamo dataset [1], an extensive repository of animations performed by various 3D virtual characters with distinct skeletons and geometry shapes. The training set we use to pre-train our skeleton aware module is the same as that used in [2], which contains 1646 motions performed by 7 characters. It’s important to note that the Mixamo dataset does not provide clean ground truth data, since many of the motion sequences suffer from interpenetration issues and semantic information loss. To mitigate this, we have carefully selected a subset of motion sequences that are both semantically clean and free of interpenetration issues for fine-tuning and testing. Our fine-tuning process involves retargeting 15 clean motions including 3127 frames, originally performed by 3 source characters, namely “Y Bot”, “X Bot”, and “Ortiz”, onto 3 target characters, including “Aj”, “Kaya”, and “Mousey”. Then we evaluate the performance of our model on the task of retargeting 30 additional motions that are previously unseen in the training set and fine-tuning sets. More details could be found in the supplementary materials.

Implementation details. The hyper-parameters λ_r , λ_c , λ_a , λ_j , λ_p , λ_s for pre-training and fine-tuning loss functions are set to 10.0, 1.0, 0.1, 1.0, 1.0, 0.1. For semantics fine-tuning, we use BLIP-2 [14] with pre-trained FlanT5-XXL

[5] large language model. To extract the semantic representation of the motion, we render animation from three perspectives, including the front view, left view and right view. The fine-tuning process takes 25 epochs with 5 clean motion sequences of the source character for each target character. During pre-training and fine-tuning, we use an Adam optimizer to optimize the retargeting network. Please refer to the supplementary materials for more details.

Evaluation metrics. We evaluate the performance of our method across three key dimensions: skeleton, geometry, and semantics. At the skeletal level, we measure the Mean Square Error (MSE) between retargeted joint positions and the ground truth provided by Mixamo, analyzing both the global and the local joint positions. At the geometric level, we evaluate the interpenetration percentage (PEN). At the semantic level, we utilize the Image-Text Matching (ITM) score, Fréchet inception distance (FID) and semantics consistency loss (SCL) as metrics. The ITM score quantifies the visual-semantic similarity between the source textual description and the rendered retargeted motion. FID is calculated between the semantic embedding distribution of retargeted motion and source motion. More details are provided in the supplementary materials.

4.2. Comparison with State of the Arts

Quantitative. In this section, we conduct a comparative analysis of our method against the state-of-the-art approaches as illustrated in Tab. 1. The baseline methods include R2ET [29], SAN [2], NKN [26] and the Copy strategy. The Copy strategy achieves the lowest local MSE because the ground truth data in the Mixamo dataset are not entirely clean, and many of them are generated by copying rotations. As a result, this strategy comes at the cost of semantic loss and interpenetration issues. SAN [2] and NKN [26] focus on skeleton-level motion features, which results in a high interpenetration rate and relatively low semantics preservation. R2ET [29] treats motion semantics as the joint distance matrix and mesh distance field, which helps it obtain better motion semantics than SAN and Copy. Nevertheless, there is still a gap between the human-designed distance matrix and the human-level semantics. Notably, our model exhibits the best interpenetration rate and semantics preservation among all methods, showcasing the capability of the proposed method in producing high-quality retargeted motions with semantics consistency.

Qualitative. In Fig. 4, we visualize the text descriptions of the motions and the qualitative comparison between the state-of-the-arts and our method. SAN [2] and Copy neglect the preservation of semantics and have severe interpenetration. R2ET [29] utilizes joint distance matrix as semantics representation and fails to capture high-level semantic information. For example, the salute motion retargeted by R2ET [29] appears more like a hand-up motion. As a comparison,

Method	MSE ↓	MSE ^{lc} ↓	Pen.% ↓	ITM ↑	FID ↓	SCL ↓
Source	-	-	4.43	0.796	-	-
GT	-	-	9.06	0.582	26.99	1.331
Copy	-	0.005	9.03	0.581	26.58	1.327
NKN [26]	0.326	0.231	8.71	0.575	27.79	1.414
SAN [2]	0.435	0.255	9.74	0.561	28.33	1.448
R2ET [29]	0.499	0.496	7.62	0.643	5.469	0.405
Ours	0.284	0.229	3.50	0.680	0.436	0.143

Table 1. Quantitative comparison with the state-of-the-arts. MSE^{lc} denotes the local MSE. ITM indicates the image-text matching score. FID is Fréchet inception distance of motion semantics. SCL is the semantics consistency loss.

Method	MSE ↓	MSE ^{lc} ↓	Pen.% ↓	ITM ↑	FID ↓	SCL ↓
SMT _{tw_s}	0.248	0.129	8.37	0.586	7.727	0.769
SMT _{tw_f}	7.798	7.083	0.44	0.432	56.53	13.29
SMT _{tw_a}	0.335	0.288	5.36	0.658	2.826	0.266
SMT _{f_{w_p}}	0.439	0.368	1.22	0.597	7.241	0.583
SMT _{f_{w_i}}	5.418	4.576	4.41	0.552	78.46	18.96
SMT _{f_{w_q}}	0.739	0.517	4.56	0.668	2.497	0.191
SMT _{Ours}	0.284	0.229	3.50	0.680	0.436	0.143

Table 2. Ablation study. SMT_{tw_s} is the network trained with only skeleton-aware pre-training. SMT_{tw_f} is the network trained with only semantics and geometry fine-tuning. SMT_{tw_a} is the network trained in one stage. SMT_{f_{w_p}} is the network fine-tuned with only the interpenetration loss. SMT_{f_{w_i}} is the network fine-tuned with image features. SMT_{f_{w_q}} is the network fine-tuned with the features of the querying transformer.

our method is able to successfully preserve high-level motion semantics leveraging the vision-language model. We observe that our approach reaches the best results among all methods, achieving more reliable semantics preservation and lower interpenetration rates. It suggests that with semantics and geometry fine-tuning, our method could effectively solve interpenetration issues together with semantics preservation.

4.3. Ablation Studies

Skeleton-aware pre-training. The proposed method can be divided into two stage: pre-training and fine-tuning. To illustrate the importance of skeleton-aware pre-training, we evaluate the network trained with only the semantics consistency loss and the interpenetration loss in Tab. 2, denoted as SMT_{tw_f}. The network trained without skeleton-aware pre-training performs worst in MSE and semantics preservation. A reasonable explanation is that the semantics consistency loss is highly non-linear, so it is important to pre-train the network at the skeletal level to provide better initial values. We also visualize qualitative results in Fig. 5.

Semantics & geometry fine-tuning. We also conduct ablation study to illustrate the importance of semantics and geometry fine-tuning in Tab. 2. We first evaluate the performance of the skeleton-aware model without fine-tuning, denoted as SMT_{tw_s}. Though it reaches the best global posi-

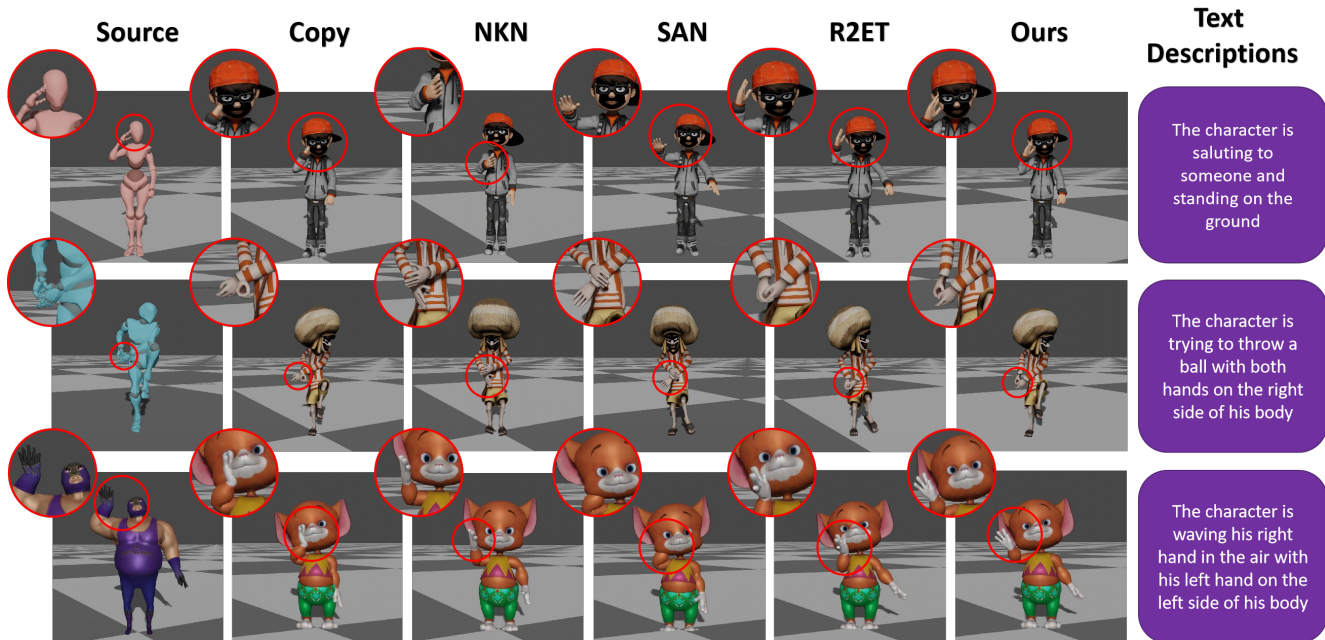


Figure 4. Qualitative comparison. The results demonstrate that our method can effectively preserve semantics while the baseline methods suffer from interpenetration or semantic information loss. From the first column to the last column are the source motion, the Copy strategy, NKN [26], SAN [2], R2ET [29], our method and text descriptions, respectively.

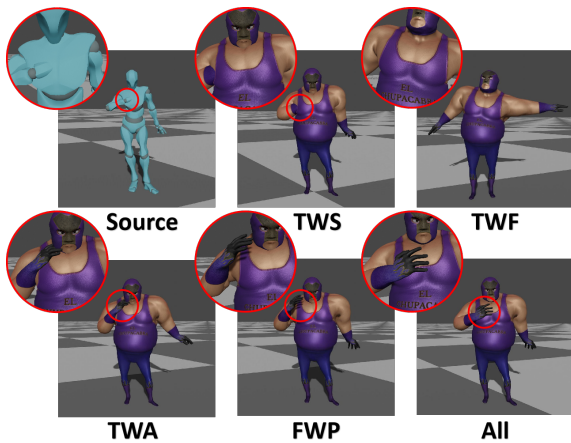


Figure 5. The qualitative comparison of ablation study between the network without fine-tuning (TWS), the network trained with only semantics and geometry fine-tuning (TWF), the network trained with all loss functions (TWA), the network fine-tuned with only the interpenetration loss (FWP) and our full model (All).

tion MSE, it suffers from interpenetration and semantic information loss because of the low-quality motion data provided by Mixamo. We next evaluate the network fine-tuned with only the interpenetration loss, denoted as SMT_{fwp} . This version results in a significant boost in terms of penetration rate. However, the gradient of interpenetration loss is only relevant with the face normals of the geometry mesh without considering the semantic information conveyed in the motion. It indicates the importance of the semantic consistency loss that makes the network reach a better balance

between interpenetration and semantics. We also try to train the network with all loss functions in one stage, denoted as SMT_{twa} . However, it is challenging for the model to acquire general knowledge of interpenetration and semantics that is suitable for every character with limited data. Therefore, training the model with skeleton-aware pre-training and fine-tuning it with semantics consistency and geometry constraints for each target character remains a more reasonable and data-efficient strategy.

Latent semantic embedding. The vision-language model used for semantic extraction can be divided into three parts: the image encoder from CLIP [22], the querying transformer and the large language model. In Tab. 2, we compare the feature outputted by the image encoder, the querying transformer and the encoder of the large language model, denoted as SMT_{fvis} , SMT_{fwq} , and SMT_{Ours} , respectively. The results show that the image feature performs worse since it is greatly affected by the appearance of the character. It indicates that with the help of the large language model, the semantic representation better focuses on the semantic meaning of the motion instead of the character’s visual appearance. Therefore, the encoder output of the large language model is more suitable for semantic embedding. More details can be found in the supplementary materials.

Prompt design. To validate the importance of guiding visual question answering, we compare the textual descriptions generated by visual question answering with and without guiding questions as well as image captioning. The re-

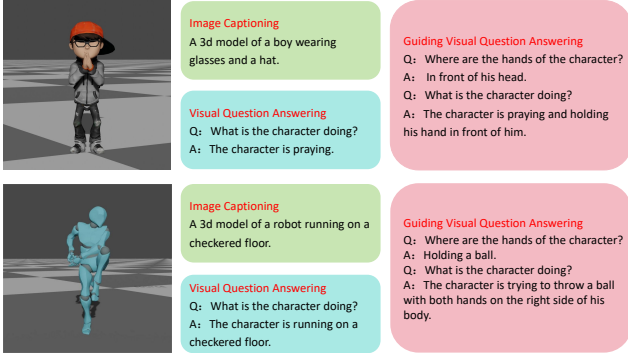


Figure 6. Text descriptions generated by different ways. The guiding visual question answering yields more comprehensive results.

Method	Quality \uparrow	Smoothness \uparrow	Semantics \uparrow
Copy	0.72	0.86	0.71
NKN [26]	0.65	0.80	0.66
SAN [2]	0.69	0.82	0.67
R2ET [29]	0.80	0.61	0.85
Ours	0.89	0.80	0.92

Table 3. User study results. We collect 100 comparisons in three aspects. Our method gets highest scores in the overall quality as well as semantics preservation.

sults in Fig. 6 indicate that using guiding questions for visual question answering yields the most comprehensive and reasonable text descriptions for motion semantics. Compared with image captioning that uses the vision-language model to generate text description directly from images, the answers from visual question answering task can be guided by the designed question to focus on motion semantics.

4.4. User Study

We conduct a user study to evaluate the performance of our method against the baseline methods. Human subjects are given 12 videos. Each video includes one source skinned motion and five anonymous skinned results. The retargeted results are randomly placed. We ask subjects to rate the results out of 1.0 in three aspects: overall quality, motion smoothness and semantics preservation. We collect a total of 100 comparisons. During the evaluation, users are required to extract semantic meaning from the source motion themselves and then evaluate the preservation of retargeted motions. In general, more than 92% of subjects prefer the retargeting results of our method.

4.5. Retargeting Motion from Human Videos

In this section, we evaluate our motion retargeting approach from human videos in the human3.6M [10] dataset. Video retargeting involves two stages: human pose estimation from video and motion retargeting. However, inaccuracies in estimating body postures may result in semantic information loss and thus accumulation of errors in the entire

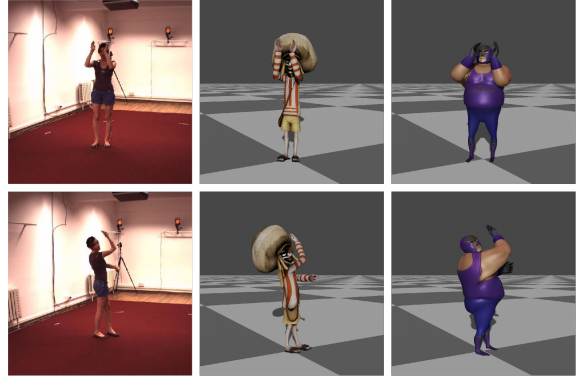


Figure 7. We retarget from human motion clips in the human3.6M [10] dataset. The retargeted motions are free from interpenetration and preserve semantics well.

retargeting process. Therefore, we first get the estimated human pose from [19]. Then we utilize the vision-language model to extract the semantic embedding of the original video and calculate the semantic consistency loss to optimize the joint angles acquired from the retargeting process directly. In Fig. 7, we show our results of motion retargeting from human videos to Mixamo characters.

5. Conclusions

In this paper, we present a novel semantics-aware motion retargeting method that leverages the capabilities of vision-language models to extract semantic embeddings and facilitate the preservation of motion semantics. This approach offers a promising solution to the challenge of lacking labelled semantic data for motion. Our proposed method involves a two-stage process that integrates skeleton-level motion characteristics and semantics-level consistency along with geometry constraints. Experimental results demonstrate that our approach excels in generating high-quality retargeted motions with semantics consistency.

Limitations. The main limitation is the performance of the vision-language model in extracting motion semantics. Without the support of motion semantic datasets of sufficient data size and quality, we rely on the model pre-trained on large image-text datasets. Although the model achieves some remarkable results in motion semantics extraction, there is still room for improvement. In addition, the projection of 3D motion into 2D images loses spatial information and affects the performance.

Future work. Compared with 2D vision-language models, 3D vision-language models have the advantage of capturing spatial relationships directly. Therefore, fine-tuning 3D vision-language models to make them more suitable for the task of motion semantics extraction is worth exploring in our future work.

Acknowledgements. This work was supported by the National Nature Science Foundation of China under Grant 62173293.

References

- [1] Adobe’s mixamo. <https://www.mixamo.com/>. Accessed: 2023-02-08. **1, 5**
- [2] Kfir Aberman, Peizhuo Li, Dani Lischinski, Olga Sorkine-Hornung, Daniel Cohen-Or, and Baoquan Chen. Skeleton-aware networks for deep motion retargeting. *ACM Transactions on Graphics (TOG)*, 39(4):62–1, 2020. **1, 2, 3, 5, 6, 7, 8**
- [3] Daichi Azuma, Taiki Miyanishi, Shuhei Kurita, and Motoaki Kawanabe. Scanqa: 3d question answering for spatial scene understanding. In *Proceedings of the IEEE/CVF Conference on Computer Vision and Pattern Recognition (CVPR)*, 2022. **4**
- [4] Kwang-Jin Choi and Hyeong-Seok Ko. Online motion retargeting. *The Journal of Visualization and Computer Animation*, 11(5):223–235, 2000. **2**
- [5] Hyung Won Chung, Le Hou, Shayne Longpre, Barret Zoph, Yi Tay, William Fedus, Yunxuan Li, Xuezhi Wang, Mostafa Dehghani, Siddhartha Brahma, et al. Scaling instruction-finetuned language models. *arXiv preprint arXiv:2210.11416*, 2022. **6, 1**
- [6] Michael Gleicher. Retargetting motion to new characters. In *Proceedings of the 25th annual conference on Computer graphics and interactive techniques*, pages 33–42, 1998. **2**
- [7] Chuan Guo, Xinxin Zuo, Sen Wang, Shihao Zou, Qingyao Sun, Annan Deng, Minglun Gong, and Li Cheng. Action2motion: Conditioned generation of 3d human motions. In *Proceedings of the 28th ACM International Conference on Multimedia*, pages 2021–2029, 2020. **3**
- [8] Chuan Guo, Shihao Zou, Xinxin Zuo, Sen Wang, Wei Ji, Xingyu Li, and Li Cheng. Generating diverse and natural 3d human motions from text. In *Proceedings of the IEEE/CVF Conference on Computer Vision and Pattern Recognition*, pages 5152–5161, 2022. **3**
- [9] Lei Hu, Zihao Zhang, Chongyang Zhong, Boyuan Jiang, and Shihong Xia. Pose-aware attention network for flexible motion retargeting by body part. *IEEE Transactions on Visualization and Computer Graphics*, pages 1–17, 2023. **2**
- [10] Catalin Ionescu, Dragos Papava, Vlad Olaru, and Cristian Sminchisescu. Human3.6m: Large scale datasets and predictive methods for 3d human sensing in natural environments. *IEEE Transactions on Pattern Analysis and Machine Intelligence*, 36(7):1325–1339, 2014. **8**
- [11] Jehée Lee and Sung Yong Shin. A hierarchical approach to interactive motion editing for human-like figures. In *Proceedings of the 26th annual conference on Computer graphics and interactive techniques*, pages 39–48, 1999. **2**
- [12] John P Lewis, Matt Corder, and Nickson Fong. Pose space deformation: a unified approach to shape interpolation and skeleton-driven deformation. In *Proceedings of the 27th annual conference on Computer graphics and interactive techniques*, pages 165–172, 2000. **3, 4, 5**
- [13] Junnan Li, Dongxu Li, Silvio Savarese, and Steven Hoi. Blip-2: Bootstrapping language-image pre-training with frozen image encoders and large language models. *arXiv preprint arXiv:2301.12597*, 2023. **2**
- [14] Junnan Li, Dongxu Li, Silvio Savarese, and Steven Hoi. BLIP-2: bootstrapping language-image pre-training with frozen image encoders and large language models. In *ICML*, 2023. **5, 1**
- [15] Kungpeng Li, Yulun Zhang, Kai Li, Yuanyuan Li, and Yun Fu. Visual semantic reasoning for image-text matching. In *ICCV*, 2019. **1**
- [16] Jongin Lim, Hyung Jin Chang, and Jin Young Choi. Pmnet: Learning of disentangled pose and movement for unsupervised motion retargeting. In *BMVC*, page 7, 2019. **1, 2, 3**
- [17] Kevin Lin, Linjie Li, Chung-Ching Lin, Faisal Ahmed, Zhe Gan, Zicheng Liu, Yumao Lu, and Lijuan Wang. Swinbert: End-to-end transformers with sparse attention for video captioning. In *CVPR*, 2022. **3**
- [18] Shichen Liu, Tianye Li, Weikai Chen, and Hao Li. Soft rasterizer: A differentiable renderer for image-based 3d reasoning. In *Proceedings of the IEEE/CVF International Conference on Computer Vision*, pages 7708–7717, 2019. **4**
- [19] Gyeongsik Moon, Hongsuk Choi, and Kyoung Mu Lee. Accurate 3d hand pose estimation for whole-body 3d human mesh estimation. In *Computer Vision and Pattern Recognition Workshop (CVPRW)*, 2022. **8**
- [20] Dario Pavllo, Christoph Feichtenhofer, David Grangier, and Michael Auli. 3d human pose estimation in video with temporal convolutions and semi-supervised training. In *Conference on Computer Vision and Pattern Recognition (CVPR)*, 2019. **3**
- [21] Zoran Popović and Andrew Witkin. Physically based motion transformation. In *Proceedings of the 26th annual conference on Computer graphics and interactive techniques*, pages 11–20, 1999. **2**
- [22] Alec Radford, Jong Wook Kim, Chris Hallacy, Aditya Ramesh, Gabriel Goh, Sandhini Agarwal, Girish Sastry, Amanda Askell, Pamela Mishkin, Jack Clark, et al. Learning transferable visual models from natural language supervision. In *International conference on machine learning*, pages 8748–8763. PMLR, 2021. **7, 2**
- [23] Guy Tevet, Brian Gordon, Amir Hertz, Amit H Bermano, and Daniel Cohen-Or. Motionclip: Exposing human motion generation to clip space. In *European Conference on Computer Vision*, pages 358–374. Springer, 2022. **2**
- [24] Guy Tevet, Sigal Raab, Brian Gordon, Yonatan Shafir, Daniel Cohen-Or, and Amit H Bermano. Human motion diffusion model. *arXiv preprint arXiv:2209.14916*, 2022. **3**
- [25] Laurens Van der Maaten and Geoffrey Hinton. Visualizing data using t-sne. *Journal of machine learning research*, 9(11), 2008. **2, 3**
- [26] Ruben Villegas, Jimei Yang, Duygu Ceylan, and Honglak Lee. Neural kinematic networks for unsupervised motion retargeting. In *Proceedings of the IEEE conference on computer vision and pattern recognition*, pages 8639–8648, 2018. **1, 2, 3, 4, 6, 7, 8**
- [27] Ruben Villegas, Duygu Ceylan, Aaron Hertzmann, Jimei Yang, and Jun Saito. Contact-aware retargeting of skinned motion. In *Proceedings of the IEEE/CVF International Conference on Computer Vision*, pages 9720–9729, 2021. **1, 2**

- [28] Zhengyuan Yang, Songyang Zhang, Liwei Wang, and Jiebo Luo. Sat: 2d semantics assisted training for 3d visual grounding. In *ICCV*, 2021. 5
- [29] Jiayu Zhang, Junwu Weng, Di Kang, Fang Zhao, Shaoli Huang, Xuefei Zhe, Linchao Bao, Ying Shan, Jue Wang, and Zhigang Tu. Skinned motion retargeting with residual perception of motion semantics & geometry. In *Proceedings of the IEEE/CVF Conference on Computer Vision and Pattern Recognition*, pages 13864–13872, 2023. 1, 2, 3, 6, 7, 8, 4
- [30] Yi Zhou, Connelly Barnes, Jingwan Lu, Jimei Yang, and Hao Li. On the continuity of rotation representations in neural networks. In *Proceedings of the IEEE/CVF Conference on Computer Vision and Pattern Recognition*, pages 5745–5753, 2019. 3
- [31] Deyao Zhu, Jun Chen, Xiaoqian Shen, Xiang Li, and Mohamed Elhoseiny. Minigt-4: Enhancing vision-language understanding with advanced large language models. *arXiv preprint arXiv:2304.10592*, 2023. 2
- [32] Ziyu Zhu, Xiaojian Ma, Yixin Chen, Zhidong Deng, Siyuan Huang, and Qing Li. 3d-vista: Pre-trained transformer for 3d vision and text alignment. *ICCV*, 2023. 4

Semantics-aware Motion Retargeting with Vision-Language Models

Supplementary Material

In this document, we provide the following supplementary content:

- Dataset Details
- Evaluation Metrics
- Implementation Details
- Semantic Attention Visualization
- Ablation Study
- Additional Results

A. Dataset Details

Test set and fine-tuning set details. We download 45 source motions of source characters including Y Bot, X Bot and Ortiz for testing and fine-tuning. More details can be found in Tab. 7. As we focus on the preservation of semantics, we choose the motions that are free of interpenetration and have obvious semantics which can be accurately described by text descriptions. To compute the MSE metric, we download the corresponding ground truth data provided by Mixamo of target characters including Aj, Kaya and Mousey. The ground truth is mainly created by copying the rotations of corresponding joints from the source character thus suffering from interpenetration and semantic loss. In order to equip our model with abundant information about geometry skinning and motion semantics, we carefully choose motions that explore the entire movement space of each source character for fine-tuning the model.

B. Evaluation Metrics

We evaluate the performance of our method across three key dimensions: skeleton, geometry, and semantics. At the skeletal level, we measure the Mean Square Error (MSE) between retargeted joint positions $\hat{\mathbf{P}}_B$ and ground truth \mathbf{P}_B provided by Mixamo, normalized by the character height h_B . We compare both the global and the local joint positions. The local MSE is calculated when the root position is aligned with the ground truth.

$$MSE = \frac{1}{h_B} \left\| \hat{\mathbf{P}}_B - \mathbf{P}_B \right\|_2^2 \quad (12)$$

At the geometric level, we evaluate the interpenetration percentage, which is calculated as the ratio of the number of penetrated vertices to the total number of vertices in each frame. A lower ratio indicates less interpenetration occurs.

$$PEN = \frac{\text{Number of penetrated vertices}}{\text{Total number of vertices}} \times 100\% \quad (13)$$

At the semantic level, we utilize the Image-Text Matching (ITM) score, Fréchet inception distance (FID) and semantics consistency loss as metrics to evaluate the semantics consistency. The task of Image-Text Matching [15] is to measure the visual-semantic similarity between an image and a textual description via a two-class linear classifier \mathcal{F}_c pre-trained in BLIP-2 [14]. To compute ITM, we first generate the textual description of the source motion with visual question answering and then compute the ITM score between the source textual description, denoted as *text*, and the rendered retargeted motion, denoted as *image*.

$$ITM = \mathcal{F}_c(\text{text}, \text{image}) \quad (14)$$

Fréchet inception distance (FID) is calculated between the semantic embedding distribution of retargeted motion and source motion. Let $\mathcal{N}(\mu_s, \Sigma_s)$ denotes the source distribution, while $\mathcal{N}(\mu_t, \Sigma_t)$ denotes the target distribution.

$$FID = \|\mu_s - \mu_t\|_2^2 + \text{tr}(\Sigma_s + \Sigma_t - 2(\Sigma_s^{\frac{1}{2}}\Sigma_t\Sigma_s^{\frac{1}{2}})^{\frac{1}{2}}) \quad (15)$$

C. Implementation Details

Training details. We use four NVIDIA 3090Ti (24*4GB) and the training process is divided into two stages. For skeleton-aware pre-training, the learning rate is set as 0.0003, the number of training epoch is set as 80 and the batch size is 16. For semantics fine-tuning, the learning rate is set to 0.0001 and batch size is 4. After 25 epoches, our model achieves state-of-the-art performance in motion retargeting and preserves the semantics of motion well. When fine-tuning our model with the interpenetration loss and the semantics consistency loss, we increase the weight of the interpenetration loss from 1.0 to 10.0 during the first 5 epochs. Because we observe that the performance of the vision-language model is unstable when there exists obvious interpenetration. And after 5 epoch, the weight goes back to 1.0. The initial hyper-parameters $\lambda_r, \lambda_c, \lambda_a, \lambda_j, \lambda_p, \lambda_s$ for pre-training and fine-tuning loss functions are set to 10.0, 1.0, 0.1, 1.0, 1.0, 0.1. The vision language model we used is BLIP-2 [14] with pre-trained FlanT5-XXL [5] large language model and large scale pre-trained vision transformer. In order to generate more comprehensive text for our prompt, we use beam search with a beam width of 5. We also set the length-penalty to 1 which encourages longer answers.

Network architecture. The motion encoder and decoder architectures consist of three layers of graph convolutions. The first two layers utilize spatial graph convolution, adopting a message-passing scheme to aggregate features from

Method	MSE ↓	MSE ^{lc} ↓	Pen.% ↓	ITM ↑	FMD ↓	SCL ↓
SMT _{fwl}	5.418	4.576	4.41	0.552	78.46	18.96
SMT _{fwq}	0.739	0.517	4.56	0.658	2.497	0.191
SMT _{Ours}	0.284	0.229	3.50	0.680	0.436	0.143

Table 4. Ablation study on semantic embedding. We compare the performance of the model fine-tuned with the image feature from CLIP [22] as semantic embedding (SMT_{fwl}), the model fine-tuned with the features of the querying transformer as semantic embedding (SMT_{fwq}) and the model fine-tuned with the features of the large language model encoder (SMT_{Ours})

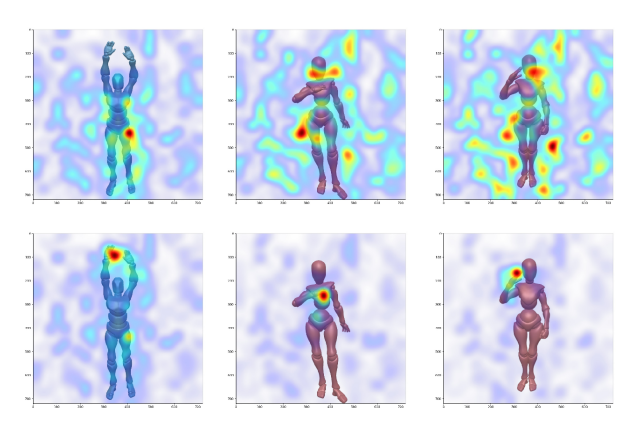


Figure 8. The cross attention map between question and image to generate semantic embedding, the first row is question without prompt and second row is question with prompt. Through guiding visual question answering, the semantic embedding concentrate on the localized regions which preserve motion semantics.

neighboring nodes as Eq. 16. The last layer is the temporal graph convolution, which maintains the same number of channels. The motion encoder receives joint rotations and positions as input and encodes them into latent motion embeddings, expanding the channels from 9 to 16 and 32. Subsequently, the motion decoder takes these latent motion embeddings as input and outputs the target joint rotations, gradually reducing the channels from 32 to 16 and 6. Additionally, the root joint positions are generated using a two-layer MLP, starting with node features from the root joint and expanding channels to 16 and 3.

$$\mathbf{x}_i' = \mathbf{x}_i + \sum_{j \in N(i)} g(\mathbf{W}_f[\mathbf{x}_i, \mathbf{x}_j, \mathbf{e}_{j,i}] + \mathbf{b}_f) \quad (16)$$

where \mathbf{x}_i is the feature of node i , \mathbf{x}_i' is the updated feature of node i , $N(i)$ is the set of neighbor nodes of node i , and $\mathbf{e}_{j,i}$ is the edge feature from node j to node i , g is the LeakyReLU function, \mathbf{W}_f and \mathbf{b}_f are learnable parameters.

D. Semantic Attention Visualization

To gain insights into the preservation of motion semantics, we visualize the attention map between the question and

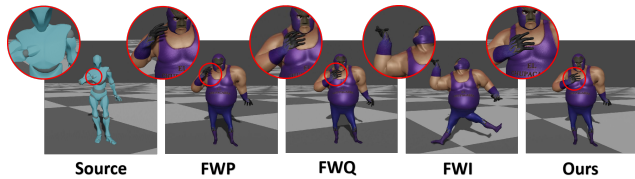


Figure 9. The qualitative comparison between the network fine-tuned without semantics (FWP), the network fine-tuned with the output of querying transformer (FWQ), the network fine-tuned with the output of image encoder (FWI), the network fine-tuned with the output of large language model encoder (Ours).

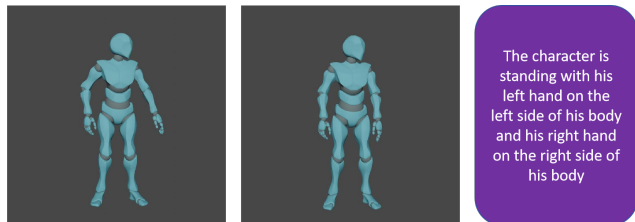


Figure 10. When the motion does not have obvious semantics, the text description can be the same while the semantic embedding from language encoder preserves the difference.

image. In Fig. 8, we illustrate how the semantic embedding accurately captures motion semantics in localized regions. This also clarifies the slight changes in the other joints of the character's skeleton with and without semantic consistency.

E. Ablation Study

Latent semantic embedding. We validate features from different levels: the output of the image encoder, the output of the querying transformer, the output of the large language model encoder. We visualize the features of three motions including Waving, Pointing and Salute with three source characters, including Y Bot, X Bot, Ortiz, using T-SNE [25] dimensionality reduction technique. The Fig. 11 shows that the features of the image encoder are clustered around characters rather than motions which indicates that the features contains more information on the appearance of the characters, while the features of the large language model encoder are clustered around motions and contains mainly motion semantics. We further use these features as semantic embedding to fine-tune our model and compute evaluation metrics in Tab. 4. The metrics and qualitative comparison indicates that appearance of character may lead to meaningless gradient for the model resulting in unnatural retargeted motion. Moreover, compared with the image features from CLIP, the features of the querying transformer and the large language model encoder focus more on relevant semantics with the help of guiding questions. Further more, We visualize the semantic embeddings outputted by VLM in Figure 12. The visualization indicates that VLM has captured rich motion semantics information, regardless

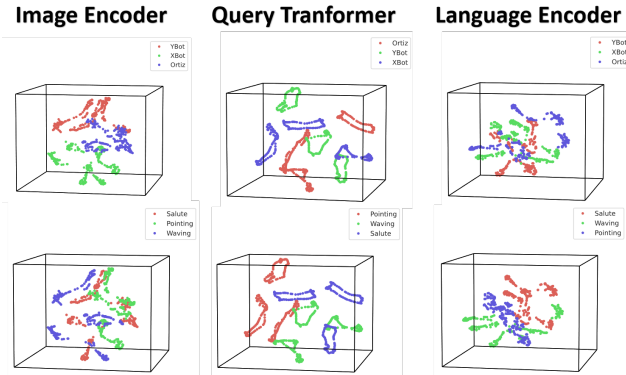


Figure 11. Features extracted from the image encoder, the query transformer and the encoder of the large language model visualized by T-SNE [25].

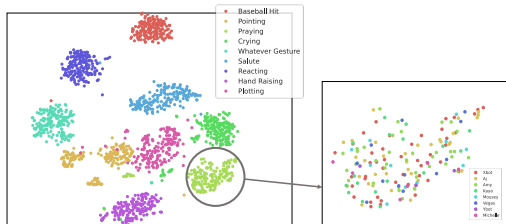


Figure 12. Visualization of semantic embedding space by t-SNE[25]. We visualize 9 motions of 8 characters with 72 sequences in total. The left figure demonstrates that frames of the same motion category are clustered. The right one shows that different characters in a single motion category are not clustered by characters.

of the appearance of the character, and is capable of guiding motion semantics preservation.

We also validate the possibility of using text descriptions as semantic embedding. But the text description of motion semantics is fuzzy and sparse. The Fig. 10 shows that during the transition phase of an action, the text descriptions remain the same. Comparing with text description, the latent features can provide dense supervision. Moreover, using text descriptions or output of decoder will bring more computation cost and higher non-linearity.

Comparison with video semantics. We compare the textual descriptions obtained from images and videos of motion sequences. The video-based vision-language model used for evaluation is SwinBert [17]. The Fig. 15 shows that although the video-based vision-language model can capture temporal information, the captured semantics is vague and lack details. The image-based vision-language model could generate more detailed and comprehensive descriptions and provide stronger supervision. Moreover, semantics of similar motions could be shared cross different motion sequence, which reduce the size of the fine-tuning set.

Performance of different numbers of views. We have conducted a new ablation in Table 5. The performance de-

Number of Views	MSE ↓	MSE ^{lc} ↓	Pen.% ↓	ITM ↑	FID ↓	SCL ↓
1 (front)	0.262	0.186	3.51	0.630	5.715	0.499
2 (left right diagonal)	0.274	0.195	3.49	0.651	2.849	0.277
3 (front, left, right)	0.284	0.229	3.50	0.680	0.436	0.143
5 (2+3)	0.286	0.233	3.50	0.681	0.433	0.141

Table 5. Quantitative comparison of different numbers of views.

Method	MSE ↓	MSE ^{lc} ↓	Pen.% ↓	ITM ↑	FID ↓	SCL ↓
NKN [26]	0.326	0.231	8.71	0.575	27.79	1.414
NKN [26] + VLM	0.392	0.308	4.44	0.665	2.687	0.223
SAN [2]	0.435	0.255	9.74	0.561	28.33	1.448
SAN [2] + VLM	0.481	0.339	5.08	0.659	2.798	0.258

Table 6. Quantitative comparison of different backbone networks.

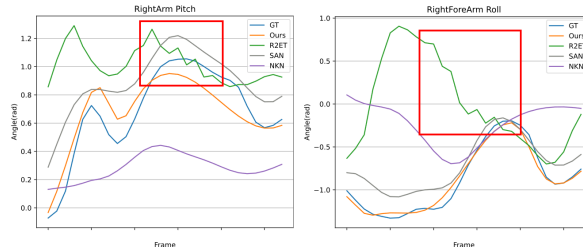


Figure 13. Example of the joint angle trajectory for the pitch and roll of the right arm.

creases to some extent with a single view due to depth information loss. Three perspectives, including the front, left and right view, can achieve fairly good results. Adding additional viewpoints after the third improves the outcome, but at a slower rate.

Ablation study of skeleton network. We have conducted a new ablation experiment in Table 6. The results show that the semantic module is applicable for different backbones and improves motion semantics preservation. The MSE metric has increased because the ground truth data in Mixamo dataset are not clean and suffer from interpenetration issues and semantic information loss [27].

F. Additional Results

More cases. We provide additional cases to validate the effectiveness of the proposed method in the task of semantics-aware motion retargeting. Fig. 16 displays a gallery of retargeted results alongside their corresponding textual descriptions. Moreover, Fig. 17, Fig. 18, Fig. 19, and Fig. 20 present the retargeted motions of “Clapping”, “Crazy”, “React”, and “Fireball” from the source character to three different target characters. These qualitative results demonstrate that our method is able to produce high-quality motion retargeting results while preserving motion semantics.

Retargeting motion from Internet videos. We also conduct experiments on motion retargeting from wild videos on the Internet in Fig. 21. The human pose is estimated using the approach proposed in [20]. Then we perform motion retargeting from the human pose to Mixamo characters.

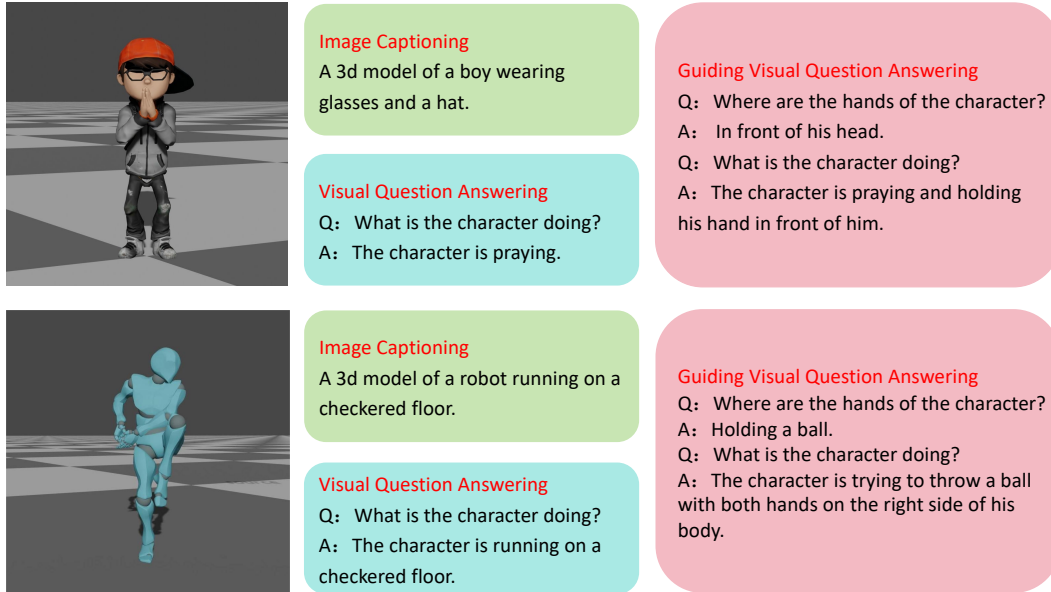


Figure 14. Text descriptions generated by different ways. The guiding visual question answering yields more comprehensive results.

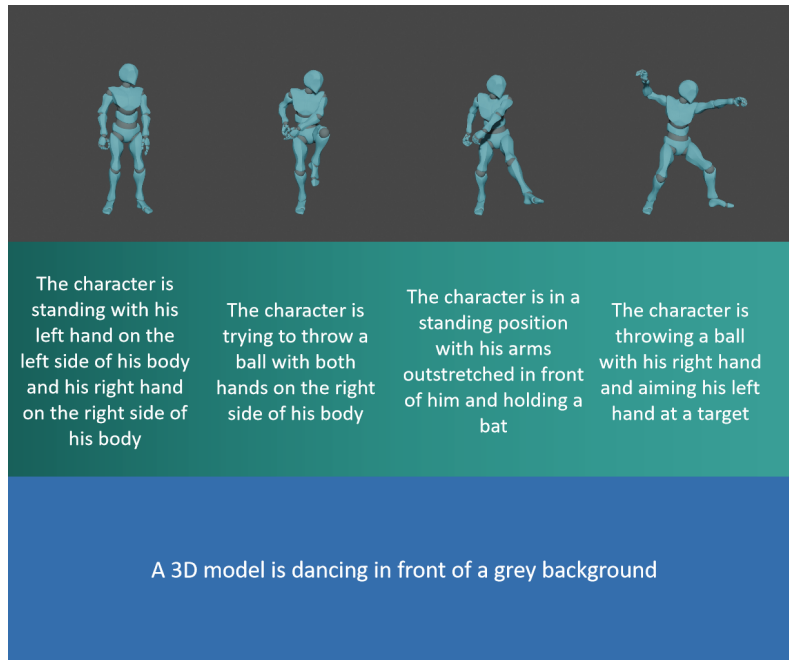


Figure 15. Text descriptions generated by the image language model and video language model. Green row is generated by image-based vision-language model. Blue row is the result of video-based vision-language model.

Considering the inherent errors in the human pose estimation, we extract the semantic embedding from the original video and apply the semantics consistency loss to further optimize the joint angles. We compare the results with and without optimization to validate the effectiveness of the semantics consistency loss. Despite the presence of some errors in human pose estimation, the retargeted motion accurately preserves the motion characteristics of the movement

in the original video.

Smoothness. We perform experiments to evaluate the smoothness of the retargeted motions. As an example, we visualize the joint angle trajectory for the pitch and roll of the right arm, and compare it with state-of-the-art methods. The Fig. 13 illustrates that our method delivers smoother motion compared to R2ET [29].

Index	Motion name	Search query	Source character	Length	Usage
1	Agreeing	Step Back Cautiously Agreeing	Y Bot	142	Test
2	Angry	Standing Angrily	Y Bot	576	Finetune
3	Baseball Hit	Baseball Base Hit	X Bot	118	Test
4	Baseball Pitching	Pitching A Baseball	Y Bot	119	Test
5	Cards	Dealing Cards	X Bot	274	Finetune
6	Charge	Point Onward Charge	Y Bot	172	Test
7	Clapping	Clap While Standing	Y Bot	36	Test
8	Counting	Counting To Five On One Hand	Y Bot	200	Test
9	Crying	Crying And Rubbing Eyes	X Bot	189	Test
10	Crazy Gesture	Crazy Hand Gesture	X Bot	151	Test
11	Defeat	Covering Face In Shame After Defeat	Y Bot	220	Finetune
12	Dismissing Gesture	Dismissing With Hand Forward	Y Bot	99	Test
13	Excited	Super Excited	X Bot	198	Finetune
14	Fireball	Street Fighter Hadouken	Y Bot	102	Test
15	Fist Pump	Pyping A Fist	Y Bot	115	Finetune
16	Focus	Shake Off Head Pain And Focus	X Bot	166	Finetune
17	Guitar Playing	Playing A Guitar	Y Bot	144	Test
18	Happy	Standing Happily	X Bot	301	Test
19	Hands Forward Gesture	Two Handed Forward Gesture	Ortiz	94	Test
20	Hand Raising	Raising A Hand	X Bot	123	Test
21	Insult	Insulting With Rude Gesture	X Bot	81	Test
22	Lead Jab	Long Body Jab	Y Bot	56	Test
23	Looking	Looking Off Into The Distance	Y Bot	241	Test
24	Loser	Showing Loser Gesture While Standing	Ortiz	99	Test
25	No	Indicating No	X Bot	151	Test
26	Padding	Padding A Single Oar Canoe	Y Bot	218	Finetune
27	Plotting	Evil Plotting	X Bot	100	Test
28	Pointing	Pointing While Seated	Ortiz	104	Test
29	Praying	Buckled Stand And Praying	Y Bot	36	Test
30	Reacting	Being Surprised And Looking Right	Ortiz	111	Test
31	Salute	Formal Military Salute	X Bot	86	Test
32	Shaking Hands 2	2 People Shaking Hands Part 2 - Male	Y Bot	132	Test
33	Smoking	Idle Smoking	Y Bot	538	Test
34	Standing Greeting	Greeting While Standing	Ortiz	154	Test
35	Thankful	Being Thankful While Standing	X Bot	91	Test
36	Taunt	Taunting Pointing At Wrist	X Bot	86	Test
37	Taunt Gesture	Taunt Gesture	Ortiz	60	Finetune
38	Talking	Asking A Question	X Bot	156	Finetune
39	Talking	Male Talking On The Cell Phone	Y Bot	145	Finetune
40	Telling A Secret	Telling A Secret	Ortiz	328	Finetune
41	Victory	Celebrating After A Win While Seated	Ortiz	184	Finetune
42	Waving	Waving With Both Hands	Ortiz	96	Finetune
43	Whatever Gesture	Whatever Gesture	Ortiz	46	Test
44	Yawn	Big Yawn While Standing	X Bot	251	Finetune
45	Yelling	Yelling In Anger	Ortiz	236	Finetune

Table 7. 45 source motion sequences of 3 characters for testing and fine-tuning.

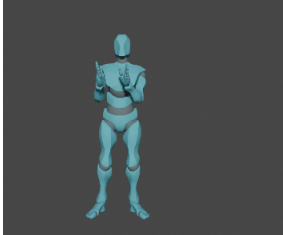
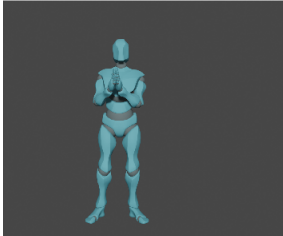
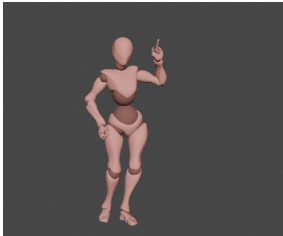
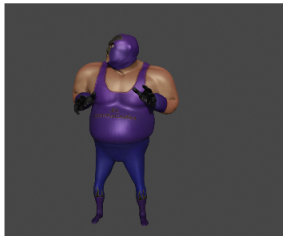
SOURCE	TARGET1	TARGET2	TARGET3	DESCRIPTION
				The character is standing with his hands positioned close together in front of his chest
				The character is praying and holding his hand up in front of him
				The character is pointing upwards with his left hand and putting his right hand on the hips
				The character is looking off to his right side and raising both hand in front of his chest
				The character is holding a ball with one hand near the chest and one hand near the raised leg

Figure 16. Snapshots of motions retargeted from the source character to three different characters and corresponding textual descriptions.



Figure 17. Snapshots of motion sequence “Clapping” retargeted from the source character to three different characters.

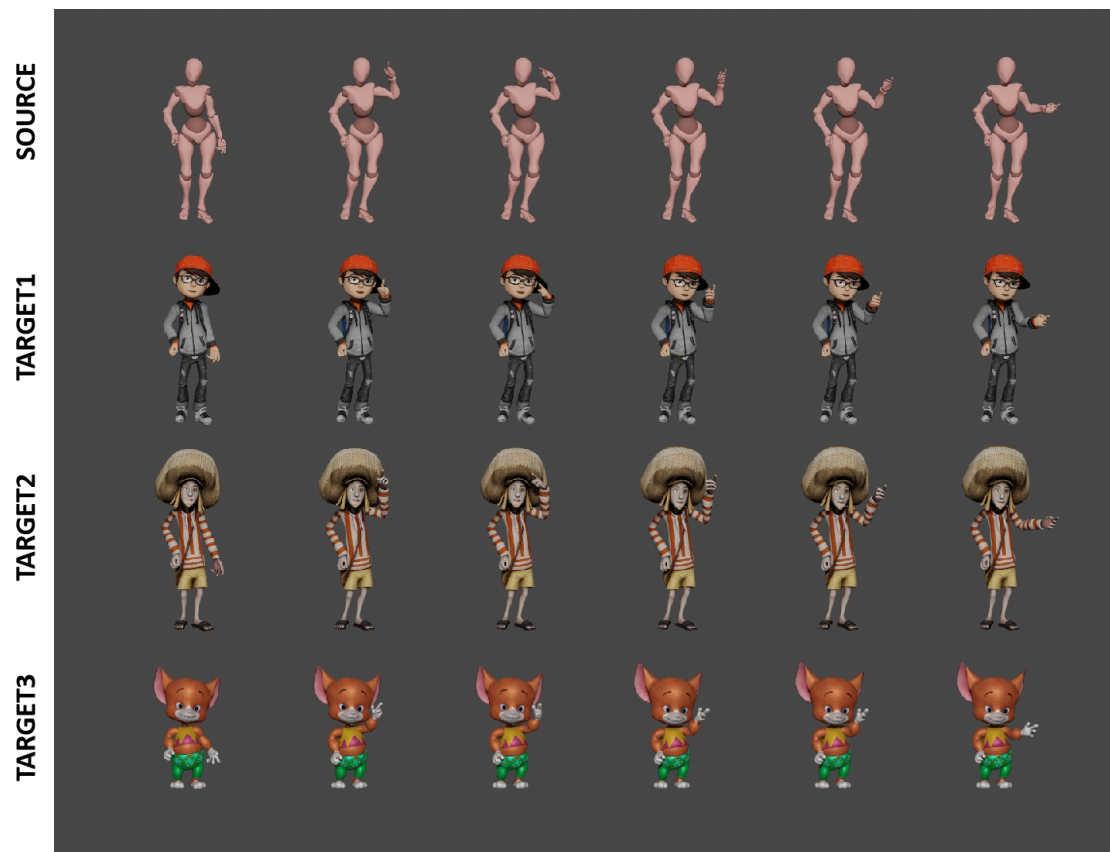


Figure 18. Snapshots of motion sequence “Crazy” retargeted from the source character to three different characters.

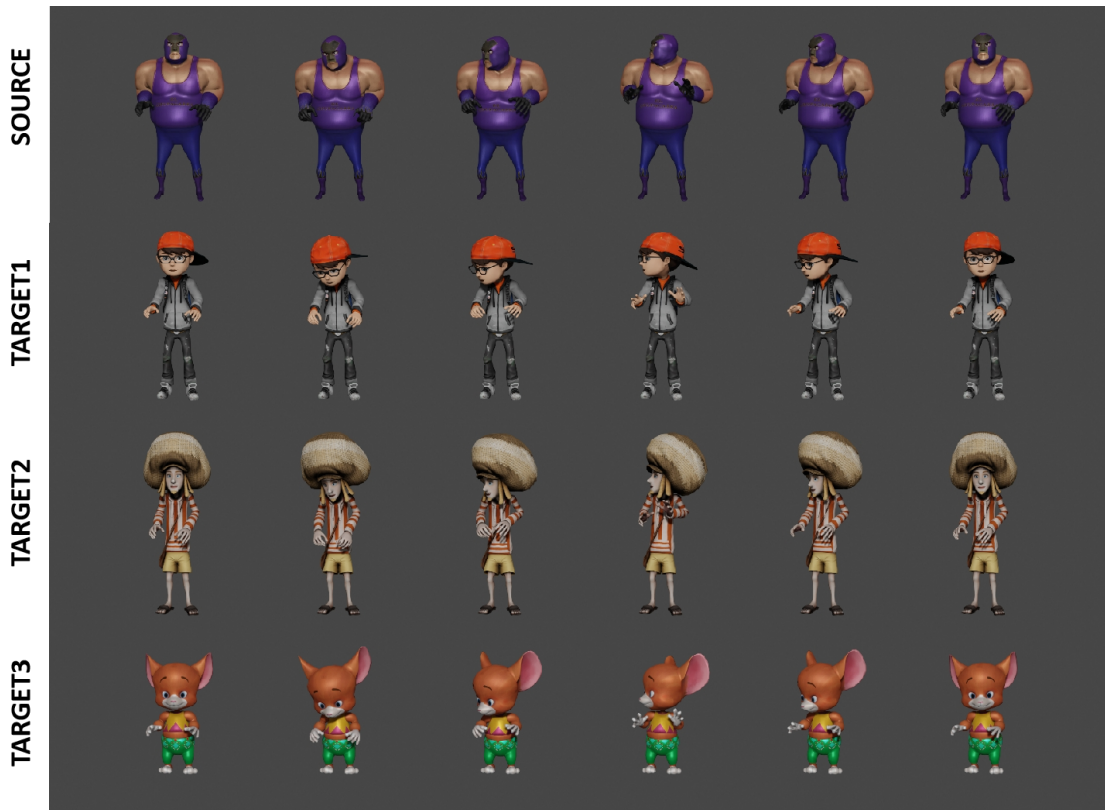


Figure 19. Snapshots of motion sequence “React” retargeted from the source character to three different characters.

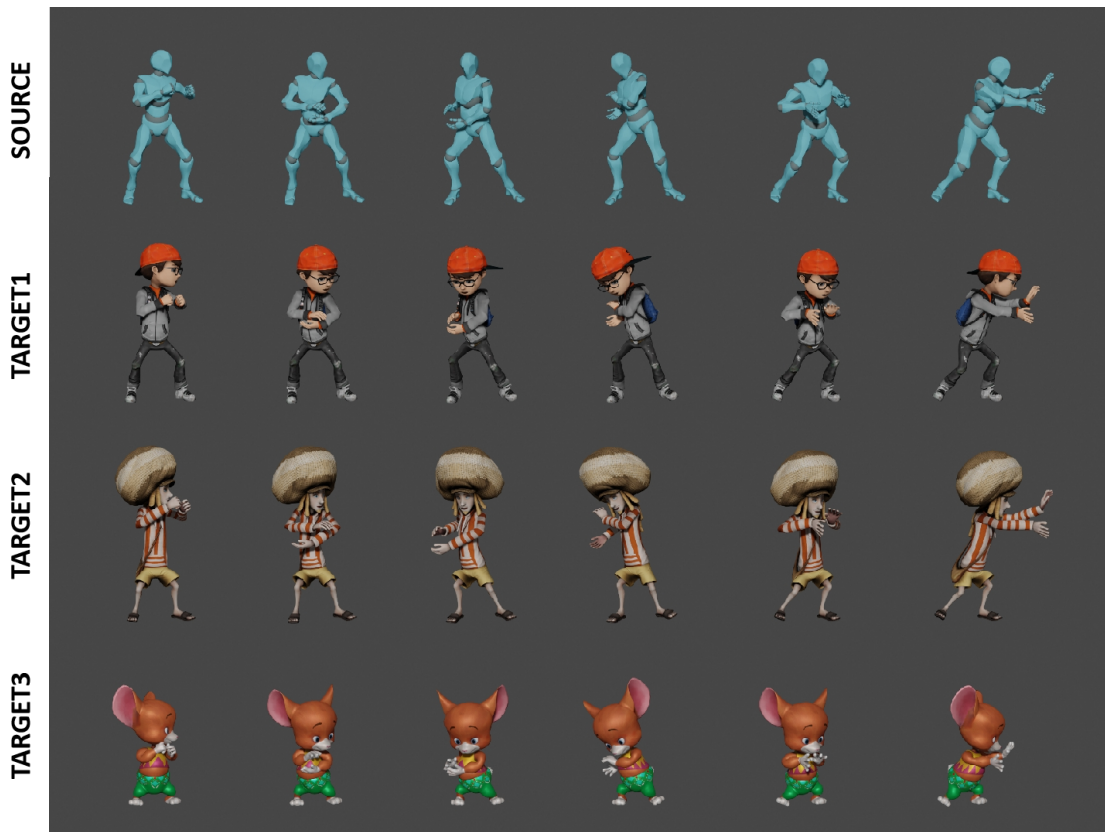


Figure 20. Snapshots of motion sequence “Fireball” retargeted from the source character to three different characters.

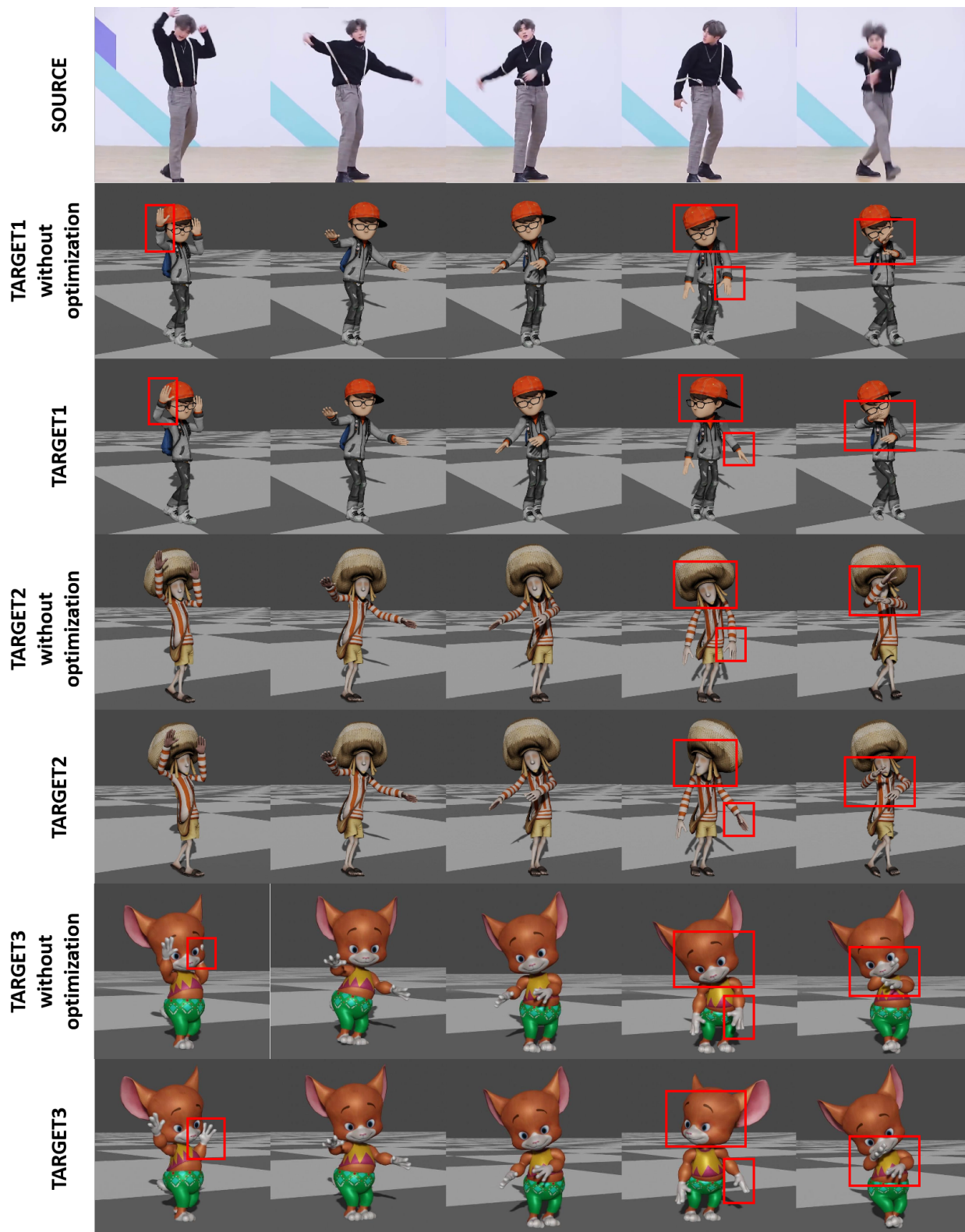


Figure 21. Snapshots of motions retargeted from the wild video on the Internet to three different characters with and without optimization.